

Reduced-Dimension Neutron Transport Code for Investigating Neutron Moderation in Inertial Confinement Fusion Nucleosynthesis Experiments

PLAS-Appelbe-2

CID: 01859936

Supervisors: Dr Brian Appelbe & Dr Aidan Crilly

Assessor: Professor Jeremy Chittenden

Word Count: 9939

**Imperial College
London**

Department of Physics
Imperial College London

Reaching for the Stars: Using Inertial Confinement Fusion to Investigate Stellar Nucleosynthesis

Scientists are developing ways to harness nuclear fusion to generate energy. Nuclear fusion, the source of energy in stars, is the process where two light nuclei combine to form a heavier nucleus, releasing a huge amount of energy. This is a potentially revolutionary technology, and a wave of successes in recent years has moved us closer to achieving this goal. Hand-in-hand with these developments comes the ability to routinely reproduce conditions seen only in the cores of stars and giant planets - if only for less than a billionth of a second. This offers physicists a unique opportunity to conduct experiments in these elusive conditions. For example, we can use the neutrons produced in fusion reactions to investigate a process responsible for the formation of chemical elements in stars: the slow neutron capture process. Physicists are particularly interested in the rates at which this process occurs when in close competition with radioactive beta decay, as understanding this would fill a gap in our knowledge regarding the evolution of stars.

At the world's largest laser system, the fusion fuel of choice is a 50:50 mixture of deuterium and tritium, two isotopes of hydrogen. This fuel is injected into a spherical capsule a few *mm* in diameter, which is rapidly heated and compressed by 192 laser beams. Once the fuel reaches thermonuclear temperatures, there are two main reactions that occur that produce high-energy neutrons. The fastest of these neutrons travel at around $50,000 \text{ km/s}$, but whilst measurements performed with these neutrons are interesting, it is ultimately more insightful to slow neutrons down to stellar-relevant energies. Since neutrons are neutral particles, the only way to slow them down is to scatter them off other particles, for which hydrogen ions are the particles of choice.

The aim of this project was to write a computer model to simulate the production and scattering of neutrons from fusion reactions so that we can better understand how to leverage the spectrum of neutrons for neutron capture experiments.

The main aim of the simulation was to find the optimum way to use hydrogen to moderate neutrons. Using the simulation, an experiment was performed where the amount of hydrogen and its location within the capsule was varied. The shape of the resulting neutron spectrum was analysed to predict the effect this would have on a measurement of the slow neutron capture process. It was found that the use of neutron moderation with current capsule technology has a detrimental impact on measurement uncertainty, suggesting a need to pursue an alternative approach.

Building on this result, the flexibility of the simulation allowed us to test additional unknown factors in the experimental method, and evaluate the effect these may have on the ability to state results with certainty. Our investigation into the impact of unknown mixing of neutron capture detectors throughout the capsule revealed that exploring the mixing of heavy ions throughout the capsule suggests that further research is needed before these experiments can become a reality.

Acknowledgements

Thanks to my project partner, and to my supervisors, Brian and Aidan.

Abstract

A reduced-dimension neutron transport code was developed to investigate neutron moderation and its application to stellar nucleosynthesis experiments using Inertial Confinement Fusion (ICF) technology, in particular neutron capture cross-section measurements. In the development of the transport model, importance was placed on the energy resolution to take advantage of the implementation of neutron scattering. With scattering treated as a probabilistic process, neutrons can scatter an arbitrary number of times, extending the knowledge of the ICF neutron spectrum below 1MeV, enabling simulations of experiments designed to measure neutron capture cross-sections.

Increased moderation of the neutron flux by the altering capsule composition aims to enhance neutron flux at stellar-relevant energies so that cross-section measurements can be performed at more appropriate energies. An investigation into neutron moderation by adding hydrogen to the capsule composition found that attempts to moderate neutron flux would hinder an experimental measurement of a neutron capture cross-section as the neutron spectrum is broadened by increased scattering, resulting in an increased measurement uncertainty

An additional investigation into dopant ion mixing indicated potential for significant error to be introduced if dopant mixing throughout the capsule is poorly understood, motivating additional research before neutron capture cross-section measurement experiments can be fielded.

The collation of results from these investigations led to the proposal of an ICF capsule design for use in cross-section measurement experiments to minimise the introduction of uncertainty into measurements.

Contents

1	Introduction	6
1.1	Nuclear Fusion	6
1.2	Inertial Confinement Fusion	6
1.3	Modelling the ICF Neutron Spectrum	7
1.4	Laboratory Astrophysics with ICF Technologies	8
1.4.1	Capsule Designs	9
1.4.2	Neutron Diagnostics	10
1.5	Objectives	11
2	Theory	12
2.1	The Neutron Transport Equation	12
2.1.1	Derivation of the Neutron Transport Equation	12
2.1.2	Approximate form of the Neutron Transport Equation	13
3	Computational Methods	14
3.1	Model Outline	14
3.2	Scattering Matrices	14
3.3	Neutron Source	16
3.4	Streaming Term	17
3.5	Target Doping Functionality	17
3.6	Construction of ODE system	18
3.7	Interpretation of the Model	19
4	Results	20
4.1	Model Verification	20
4.1.1	Comparison to Analytic Solution	20
4.1.2	High-Energy Behaviour	21
4.1.3	Streaming-Term Behaviour	22
4.2	Investigation Results	23
4.2.1	Capsule Design and Fusion Fuel Investigation	23
4.2.2	Investigation into Neutron Moderation	24
4.2.3	Investigation of Experimental Procedure for Cross-Section Measurements	27
5	Discussion	30
5.1	Discussion of Results	30
5.1.1	Capsule Design and Fusion Fuel Investigation	30
5.1.2	Neutron Moderation Investigation	30
5.1.3	Target Mixing Investigation	31
5.1.4	Proposal of Experimental Design	32
5.2	Limitations of the Model	33
6	Conclusions	34
6.1	Future Work	34

7 Appendix	35
7.1 Access to Code	35

1 Introduction

1.1 Nuclear Fusion

Nuclear fusion is the process by which two light nuclei combine to form a heavier nucleus. The products, being more stable than the reactants, have a smaller total mass. The mass difference is accounted for by the release of energy, described by Einstein's famous mass-energy relation, $E = mc^2$. Fusion energy solutions are based on thermonuclear fusion, using high temperatures to give reactants the energy required to undergo fusion reactions. The thermal energy distribution of reactants in thermal equilibrium is given as a function of particle velocity by the Maxwell-Boltzmann distribution

$$f(v) = 4\pi v^2 \left(\frac{m}{2\pi k_B T} \right)^{\frac{3}{2}} e^{-\frac{mv^2}{2k_B T}} \quad (1)$$

where v is the particle's velocity, m is its mass, T is the thermodynamic temperature and k_B is the Boltzmann constant. For fusion reactions to occur, a high enough temperature is required such that ions in the upper tail of this distribution have enough energy to fuse. As shown in Fig.1, the fusion of deuterium and tritium has a large cross-section that peaks at a relatively achievable energy of 64keV . It is widely agreed upon that a 50:50 mixture of deuterium and tritium (DT) is the optimum fuel for an energy solution [1], where the temperature required for fusion is around 10keV (100 million degrees Celsius). At such extreme temperatures, the fusion fuel becomes a plasma, a quasi-neutral ionised gas that exhibits collective behaviour and is often referred to as the 4th state of matter. All known structural materials melt at such temperatures, so novel approaches must be taken to confine any plasma of fusion fuel for long enough for sufficient energy to be released. There are two main approaches to the confinement of plasmas. Magnetic confinement fusion (MCF) uses magnetic fields to confine a low-density, high-volume plasma for extended periods of time, enabling a constant thermonuclear burn to be sustained [2], [3], [4]. Rather than using an external source of confinement, inertial confinement fusion (ICF) relies on the inertia of the plasma. The plasma can then only be confined for the time it takes for a sound wave to travel the radius of the plasma. Such short confinement times mean that any successful energy solution using ICF will necessarily be a pulsed process, where small pellets of dense fuel are burnt periodically [2].

1.2 Inertial Confinement Fusion

The aim of ICF is to achieve ignition of a spherical capsule containing a few mg of fusion fuel. Ignition occurs when the heating of the fuel due to the products of fusion reactions exceeds all energy losses. This statement is given mathematically by the Lawson Criteria

$$n\tau_e \geq \frac{12k_B T}{\langle \sigma v \rangle E_{D-T}} \quad (2)$$

where n is the ion number density, τ_e is the energy confinement time, σ is the fusion cross-section, v is the relative velocity of the reactants, and $\langle \rangle$ denotes averaging over the Maxwellian velocity distribution in (1) at an energy of $k_B T$ [6].

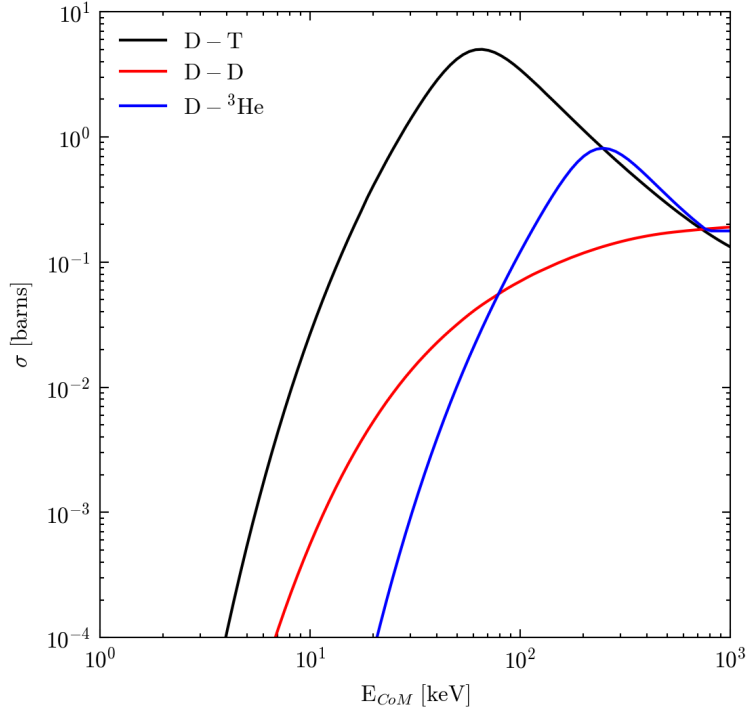


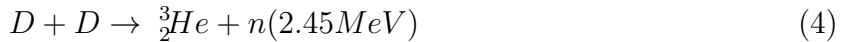
Figure 1: Reaction cross-sections for relevant fusion reactions. DT fusion has the largest cross-section, peaking at 64keV, making it the favoured reaction for a fusion energy solution. Data taken from ENDF [5].

Fusion reactions are triggered by rapidly compressing and heating a capsule until the necessary conditions are met. This implosion process is typically driven by high-power radiation. The specific heat of a DT plasma means that the implosion of a homogeneous sphere would require millions of joules of energy. This is not acceptable for an energy solution. Instead, only a small fraction of the fuel is heated to thermonuclear temperatures and the thermonuclear burn can then propagate into the surrounding fuel [7]. This approach is called hotspot ignition, and is a central feature of current ICF experiments, such as those performed at the National Ignition Facility (NIF).

NIF, at the Lawrence Livermore National Laboratory in California houses the world's largest laser system, which is used to conduct ICF experiments [8]. NIF began performing experiments into fusion energy in 2011, and has made considerable progress in recent years. In August 2021, NIF produced the first burning plasma, and in December 2022 they achieved ignition, demonstrating that a large neutron yield can routinely be achieved [9], [10].

1.3 Modelling the ICF Neutron Spectrum

In deuterium-tritium fusion, there are three reactions that produce neutrons





Reactions (3) and (4) produce neutrons at specific energies, whereas reaction (5) has three products, and so these neutrons are instead produced with a spectrum of energies [2]. Whilst these reactions suggest that the majority of neutrons are produced at single energies, the thermal distribution of ions due to their temperature means that neutrons are produced with a Gaussian distribution centered at the energies given in (3) and (4) [11]. Neutrons can also scatter off fuel ions, reducing their energy and introducing structure into the neutron energy spectrum.

The behaviour of neutrons travelling through a medium with which they can interact is described by the neutron transport equation. Solving the neutron transport equation yields the spatial and temporal evolution of a population of neutrons [12]. Exact solutions are typically not possible for any physical system, making it necessary to adopt various approximations and utilise numerical methods to find solutions. The most common approach to modelling the ICF neutron spectrum is to use a Monte Carlo approach [13]. This approach generates a set of neutron histories by tracking individual neutrons through collisions and interpreting interaction cross-sections as probabilities of interaction outcomes [12]. There is an inherent limit on the number of scattering events considered for each neutron, limiting accuracy below 1MeV . Another approach is to adopt a discrete ordinates method, in which space and energy are discretised. This approach was used by Crilly in [14], [15], in conjunction with an inverse-ray tracing method to post-process hydrodynamic simulations of NIF capsule implosions to generate synthetic neutron diagnostic data. These methods have limited accuracy below a certain energy threshold. The inverse ray-tracing method was used to generate synthetic primary and down-scattered neutron images for measurements of areal density. To do this, primary neutron spectra are calculated using an analytic model. Then, elastic scattering is calculated using tabulated energy-dependent cross-sections taken from the ENDF database. This approach performs ray-tracing in 3D, meaning that it can be used to model realistic implosion scenarios where asymmetries in the implosion process and capsule construction cause bulk fluid velocities. This allows the effects of these asymmetries on synthetic diagnostics to be investigated, with the aim of applying the knowledge gained to experimental diagnostics fielded at NIF. The main drawback of such a model is that its computational complexity limits scattering to a single event per neutron. This limits the accuracy of the model below 10MeV , as below this threshold the contribution of multiple-scattered neutrons becomes significant. Below 1MeV , this model is unable to make predictions, as a neutron must undergo multiple scattering events to be moderated down to such energies [16].

1.4 Laboratory Astrophysics with ICF Technologies

Whilst the primary goal of ICF research is a fusion energy solution, it has also led to the development of unique conditions on Earth, giving us a platform on which to perform experiments in high energy density (HED) plasma conditions similar to those found in stars. Combining these extreme conditions with a bright neutron source provides an opportunity to probe a key component of stellar nucleosynthesis: the slow neutron capture process.

The slow neutron capture process (s-process) takes place in the helium-burning layers

of low-mass asymptotic giant branch stars and in the helium-burning and carbon-burning layers of massive stars [17], [18]. It is responsible for the synthesis of half of the abundance of all elements between iron ($A = 26$) and bismuth ($A = 83$), producing elements that lie on the ‘stability valley’ seen on the chart of nuclides in Fig.2. Stable nuclei are formed via this process as the rate of neutron capture is typically slower than the rate of β -decay [19], [20]. Regions in atomic mass where these competing processes have similar rates are known as branch points, and the exact balance between capture and decay is an important factor in stellar evolution models [21], [22]. This is an area of ongoing research, and a detailed understanding of the interplay at branch points may be gained by considering how these processes occur in excited nuclei [21], [23].

Measurements of neutron capture cross-sections are possible, and have been performed at accelerator facilities [19], [24]. Whilst measurements of this nature are useful for their low background, the ambient conditions in the solid target mean that nuclei are surrounded by bound electrons. In contrast, electrons occupy degenerate states under stellar conditions [25]. An alternative method using ICF technologies can offer a solution to this discrepancy, as well as presenting additional advantages over an accelerator-based approach. The high energy density environment inside a capsule means that electrons do not occupy bound states, and so less extrapolation is required to apply results to stellar conditions [26], [27]. In addition to this, the HED environment means that excited nuclear states may be occupied, allowing for investigation of processes where excited nuclear states play an important role, such as at branch points of the s-process [28], [29]. A third benefit is that the intense neutron flux created at NIF reduces the time required for a measurement, meaning processes involving radioactive isotopes can be studied, a challenging feat at an accelerator [25].

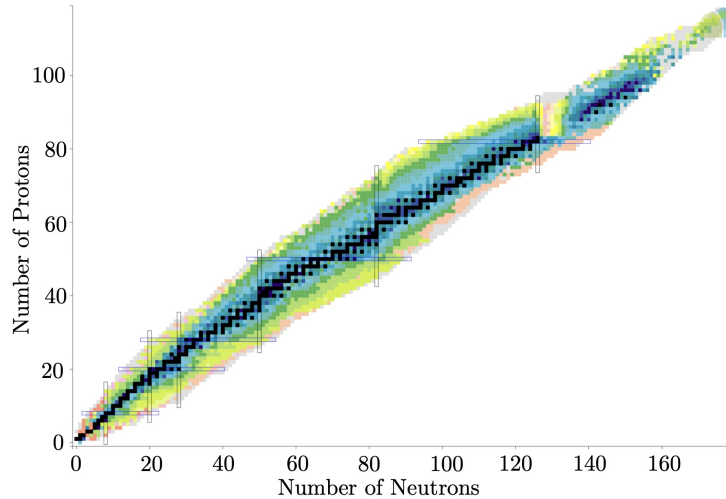


Figure 2: Chart of Nuclides, where darkness of colour indicates lifetime. The valley of stability is seen in the black line through the centre.

1.4.1 Capsule Designs

NIF’s capsule designs are an impressive feat of engineering, and are the subject of continuous development. Only the core design criteria are important for this work, and there are two

designs of interest.

The first of these is an ignition-focused capsule. These are typically high density carbon capsules (although other materials such as beryllium, plastic and glass have previously been used) around 2mm in diameter filled with a cryogenic DT solid fuel shell with a central DT gas fill [30].



Figure 3: (Left) Polished beryllium ignition capsule used at NIF. Taken from [31]. (Right) Plastic polar direct-drive capsule used at NIF. Taken from [32].

The second capsule type of interest is a polar direct-drive exploding pusher (PDXP) capsule. These are $3 - 4\text{mm}$ diameter plastic capsules typically filled with DT vapour [32], [33]. The aim of using these capsules is not to achieve ignition, but to have improved hydrodynamic stability by avoiding the mixing of the capsule shell with the fuel [34]. This is achieved through low to moderate convergence ratios (related to density increase), reducing the impact of asymmetries, and utilising shock-heating to reach thermonuclear temperatures [35]. For a direct-drive approach to be fielded at NIF, the target must be compatible with the indirect-drive laser configuration used at NIF, and so defocussed lasers are used to compensate for the drive asymmetry. A key advantage of this capsule type is that it can produce usable neutron yields at relatively low laser energies that are often below the damage threshold for NIF optics [32], [36].

1.4.2 Neutron Diagnostics

NIF has a ‘comprehensive suite’ of neutron diagnostics that are used to infer plasma properties and diagnose implosion performance [9]. Of particular interest is the suite of radiochemical diagnostics, which are used to count radionuclides. Radionuclides are produced when neutrons emitted from fusion reactions undergo nuclear reactions with radiochemical detectors placed either in, or near the capsule [37]. There are two systems developed at the Lawrence Livermore National Laboratory that can dope atoms to serve as radiochemical detectors to the inner surface of NIF capsules [38]. These are called ANDARIST and VORCAN [25].

There are two main diagnostic tools used for the collection and counting of radionuclides. The first of these is the Radiochemical Analysis of Gaseous Samples (RAGS) apparatus, which collects gaseous products produced during an experiment [38], [37]. After an experiment, gases are pumped out of the chamber and transported to the RAGS apparatus where isotope ratios are counted using spectroscopic techniques [25], [39]. The second is the solid radiochemistry (SRC) diagnostic, used to collect solid debris from experiments. Pure metal discs (typically tantalum or vanadium) 2 inches in diameter are placed 50cm from the target chamber centre, each one taking up $1/10,000$ of solid angle [39].

1.5 Objectives

The aim of this work was to develop a computational model to predict the ICF neutron spectrum, with particular focus on the spectrum below 1MeV for its relevance to astrophysical scenarios. To achieve this, the implementation of neutron scattering in the transport model must not place an upper bound on the possible number of scattering events per neutron. This should be done by probabilistically scattering neutrons at each computational time-step. The neutron transport equation and approximations applied are covered in section 2. The model had to include the ability to specify the structure and composition of the ICF capsule, to include typical fusion fuels, ablator materials, and additional materials for the purpose of moderation of the neutron flux. The model also had to include the ability to replicate the use of techniques such as VORCAN and ANDARIST at NIF, allowing for the addition of heavy ions to the capsule for use in nucleosynthesis experiments. Computational simplicity was a priority as the initial investigations performed in this work largely consisted of parameter scans over a number of variables. Development of the model is covered in section 3.

After the development of the model, its predictions were verified through comparison to both analytic and simulation results. These comparisons were done in the high energy regime ($> 1\text{MeV}$) where the neutron spectrum is well-known.

The model was used to investigate nucleosynthesis experiments at NIF. The primary goal was to investigate moderation of neutron flux to enable the measurement of cross-sections at stellar-relevant energies. The model was also used for additional investigations into capsule and fuel types, and to test the validity of the experimental procedure for performing cross-section measurements at NIF. Validation of the model and investigation results are presented in section 4.

2 Theory

2.1 The Neutron Transport Equation

The neutron transport equation is an integro-differential Boltzmann-like equation that describes the temporal and spatial evolution of a population of neutrons travelling through a medium with which they can interact. Neutrons are considered to be point particles, being described entirely by their position and momentum. This approximation holds since the de Broglie wavelength of a neutron at typical ICF energies is several orders of magnitude smaller than its typical mean free path. Interactions of neutrons with nuclei are considered to be described entirely by their total and differential cross-section.

2.1.1 Derivation of the Neutron Transport Equation

Consider a packet of neutrons, defined as the probable number of neutrons in a volume element dV with energies between E and $E + dE$, travelling in directions between Ω and $\Omega + d\Omega$, which is given by

$$N(\mathbf{r}, \Omega, E, t) dV d\Omega dE \quad (6)$$

where N is the neutron angular density. In a time Δt , there are three mechanisms by which this probable number may change:

1. Some number of neutrons may scatter, causing a change to their trajectory, Ω , and energy E , resulting in them being removed from the packet. The number of neutrons remaining is given by

$$[1 - n\sigma v \Delta t] N(\mathbf{r}, \Omega, E, t) dV d\Omega dE$$

where n is the number density of some particle species with scattering cross-section σ , and v is the speed of a neutron with energy E .

2. Some number of neutrons may enter the packet as a result of collisions within other packets. This number of neutrons is given by

$$\left[\iint n \frac{d^2\sigma}{dE' d\Omega'} v' N d\Omega' dE' \right] dV d\Omega dE \Delta t$$

where $\frac{d^2\sigma}{dE d\Omega}$ is the double differential cross-section of the scattering species.

3. Neutrons may enter the packet due to some neutron source. This is given by

$$Q \Delta t dV d\Omega dE$$

Adding these terms together and cancelling where possible gives

$$\begin{aligned}
& N(\mathbf{r} + \boldsymbol{\Omega}v\Delta t, \boldsymbol{\Omega}, E, t + \Delta t) \\
&= [1 - n\sigma v\Delta t] N(\mathbf{r}, \boldsymbol{\Omega}, E, t) + \left[\iint n \frac{d^2\sigma}{dE'd\boldsymbol{\Omega}'} v' N d\boldsymbol{\Omega}' dE' \right] \Delta t + Q\Delta t. \tag{7}
\end{aligned}$$

Rearranging, then dividing by Δt and taking the limit of $\Delta t \rightarrow 0$ gives

$$\begin{aligned}
& \lim_{\Delta t \rightarrow 0} \left[\frac{N(\mathbf{r} + \boldsymbol{\Omega}v\Delta t, \boldsymbol{\Omega}, E, t + \Delta t) - N(\mathbf{r}, \boldsymbol{\Omega}, E, t)}{\Delta t} \right] \\
&= -N(\mathbf{r}, \boldsymbol{\Omega}, E, t)n\sigma v + \iint n \frac{d^2\sigma}{dE'd\boldsymbol{\Omega}'} v' N d\boldsymbol{\Omega}' dE' + Q \tag{8}
\end{aligned}$$

where the term on the left-hand side is the co-moving derivative, defined by $\frac{D}{Dt} = \frac{\partial}{\partial t} + \boldsymbol{\Omega} \cdot \nabla$. Rewriting using the co-moving derivative allows for a transformation from the rest frame of the neutron packet to the laboratory rest frame. Rewriting in terms of neutron angular flux, $\psi = vN$ gives the standard form of the neutron transport equation

$$\frac{1}{v} \frac{\partial \psi}{\partial t} + \boldsymbol{\Omega} \cdot \nabla \psi + n\sigma\psi = n \iint \frac{d^2\sigma}{dEd\boldsymbol{\Omega}} \psi dE d\boldsymbol{\Omega} + Q. \tag{9}$$

2.1.2 Approximate form of the Neutron Transport Equation

To the standard form of the neutron transport equation, (9), approximations must be applied so that it is of a form that can be solved numerically without prohibitive computational times, and with the discretisation of the phase-space such that experimental data can be used to inform various physical processes.

Angular dependence is removed by integrating over angular direction, $\boldsymbol{\Omega}$, and spatial averaging is applied by integrating over volume. This gives

$$\frac{1}{v} \frac{d\phi}{dt} + \iint \boldsymbol{\Omega} \cdot \nabla \psi dV d\boldsymbol{\Omega} + n\sigma\phi = n \int \frac{d\sigma}{dE} \phi dE + S \tag{10}$$

where $S = \iint Q dV d\boldsymbol{\Omega} =$, and where $\phi = \iint \psi dV d\boldsymbol{\Omega}$ is a neutron flux per unit energy. The partial derivative on the left-hand side of (9) has been replaced with a total derivative as ϕ is only a function of time.

The following approximation is applied to the second term on the left-hand side

$$\iint \boldsymbol{\Omega} \cdot \nabla \psi dV d\boldsymbol{\Omega} = \frac{1}{L}. \tag{11}$$

This approximation is applied without physical justification, and has been applied because it gives the simplest form of the term that maintains correct dimensionality. Further rearranging gives

$$\frac{d\phi}{dt} = \left[\frac{-v}{L} - n\sigma v + nv \int \frac{d\sigma}{dE} dE \right] \phi + vS \tag{12}$$

which is the form of the neutron transport equation used in the model developed for this work.

3 Computational Methods

3.1 Model Outline

A reduced-dimension multigroup neutron transport code was developed that solves a system of coupled neutron transport equations for computational cells (referred to as layers) that mirror the composition of an ICF capsule. Access to the code can be found in the appendix.

The term multigroup refers to the discretisation of energy, which reduces the computational power required to solve the transport and simplifies the implementation of total and differential cross-section data. Typical results presented in this work use 500 energy bins from $10eV$ to $16MeV$ with logarithmic binning. Logarithmic binning has the advantage of increased resolution at low energies, but linear binning is used where appropriate, such as for comparison to published results.

The model solves (12), as derived in section 2.1.1. To improve the performance of the model, this equation is rearranged such that it can be implemented using matrix multiplication

$$\frac{d\phi}{dt} = \left(\frac{-v}{L} + M\right)\phi + vS. \quad (13)$$

These matrices, given by M , are formed by the addition of the terms $-nv\sigma$ and $nv \int \frac{d\sigma}{dE} dE$, and are referred to as ‘scattering matrices’.

3.2 Scattering Matrices

Each scattering matrix contains all the information required to implement the scattering of neutrons by plasma ions within a single computational cell. Scattering matrices are constructed from total and differential cross-sections of the relevant neutron interactions such that neutrons are transferred between energy bins, replicating the change in a neutron’s kinetic energy due to an interaction with an ion. Elastic scattering describes a neutron-ion interaction where the sum of the particles’ kinetic energies is conserved. By contrast, inelastic scattering describes interactions where kinetic energy is not conserved, where neutron break-up of ions are an example.

Total cross-sections give the probability that a given interaction will occur. In this work, total cross-section refers to the integral of the differential cross-section rather than the sum of cross-sections for various interactions, and the term cross-section refers specifically to the microscopic cross-section. Thus a cross-section, typically measured in barns, can be interpreted as a characteristic area presented by an ion. The discretised total cross-section gives the probability that a neutron in a given energy bin will scatter. Differential cross-sections give the probability that a neutron will be scattered by some scattering angle. In the case of elastic scattering, there is a one-to-one functional dependence between scattering angle and outgoing neutron energy, and so the differential cross-section can be given as a probability for a neutron to be scattered from a given incoming energy to some outgoing energy. In the case of inelastic scattering, double differential cross-sections give the probability that a neutron will be scattered by a given angle, and will continue with a given energy. Angular dependence is integrated out, as shown in (10), to give a differential cross-section, and so its

interpretation is the same as for elastic scattering. The discretised version of the differential cross-section gives the probability that a neutron will be transferred from one energy bin to another.

Total and differential cross-section data is loaded using the Python package NeSST (Neutron Scattered Spectra Tool) [40]. NeSST can be used to produce singly-scattered neutron spectra for ICF experiments as used in [15], [41]. This model will only make use of NeSST as a unified tool to access total and differential cross-section data. Total and differential cross-sections for elastic scattering by deuterium and tritium are taken from ENDF [5]. Inelastic cross-sections are taken from either CENDL or ENDF nuclear databases [42].

A scattering matrix is constructed for each layer (computational cell) of the capsule according to

$$M_{scattering} = \sum_x n_x v_i \left[\int \frac{d\sigma_x}{dE_i} dE_j - \sigma_x \right] \quad (14)$$

where E_i is incoming energy, E_j is outgoing energy and x denotes each neutron-ion interaction for the ion species specified in the capsule composition.

A scattering matrix is a square matrix of size $n \times n$, where n is the number of energy bins. For each interaction, the negative of the total cross-section is added to the diagonal of the scattering matrix. This implements the probabilistic removal of a neutron from a given energy bin due to it being scattered. Then, the corresponding normalised differential cross-section (multiplied by outgoing energy bin widths to account for the approximation of the integral in (14) by a sum) is added to the matrix. The differential cross-section is only non-zero below the leading diagonal of the matrix, implementing the down-scattering of neutrons through the probabilistic introduction of neutrons removed by the total cross-section to some lower energy bin. Finally, as given in (14), the scattering matrix is multiplied by the number density of the ion species and by neutron velocity at each energy bin.

The normalisation of the differential cross-section is given by the following process:

1. Prevent scattering below the lowest outgoing energy bin. This is the case for

$$\alpha E_i < E_{j,min} \quad (15)$$

where $\alpha = (\frac{N-1}{N+1})^2$ with N being the atomic mass of the scattering ion [12]. To achieve this, the integral of the differential cross-section below the lowest outgoing energy bin is added to the lowest outgoing energy bin. In this respect, the lowest energy bin acts to collect neutrons to preserve neutron conservation.

2. Ensure that for every neutron scattered out of an energy bin, a neutron is introduced to another energy bin to preserve neutron conservation. This is done by enforcing that the integral over the differential cross-section with respect to outgoing energy is equal to the total cross-section at each incoming energy. This statement is given by

$$\sigma(E_i) = \int \frac{d\sigma}{dE_i} dE_j = \sum_{E_j} \frac{d\sigma}{dE_i} \Delta E_j \quad (16)$$

where Δ denotes bin widths. Since energy has been discretised, the integral is approximated by a sum over outgoing energy.

3. Since inelastic scattering implements neutron break-up reactions of fuel ions, it must be normalised such that two neutrons leave an interaction for every neutron that scatters.

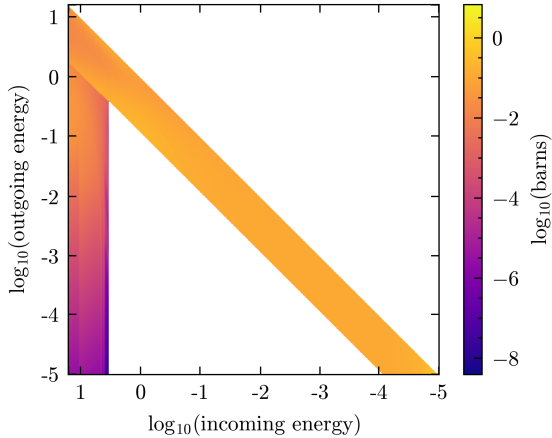


Figure 4: Matrix representation of the differential cross-sections for elastic and inelastic scattering of neutrons by deuterium ions. Elastic scattering differential cross-section is seen in the diagonal stripe. Inelastic differential cross-section is seen on the far left.

3.3 Neutron Source

In the neutron transport equation, source terms are used to describe any neutron source that is independent of neutron density. In this case these are fusion reactions. There are three reactions that produce neutrons, given in (3),(4),(5). DT and DD reactions produce neutrons at 14MeV and 2.45MeV respectively, with the kinetic energy of the reactant ions causing a thermal broadening of the neutron production energy spectrum [11]. DT and DD neutron production spectra are taken from NeSST [40], and are constructed using Ballabio's spectral moments, where reactivities are taken from [43], [44].

The neutron production rate is assigned a Gaussian time-dependence, replicating typical burn widths measured at NIF and Omega using Gamma Ray History diagnostics [45], [46]. Burn widths are typically reported as a FWHM of a gaussian burn. This burn is implemented in the model as a Gaussian with a maximum occurring at $t = 3\sigma$ where $\text{FWHM} \approx 2.4\sigma$.

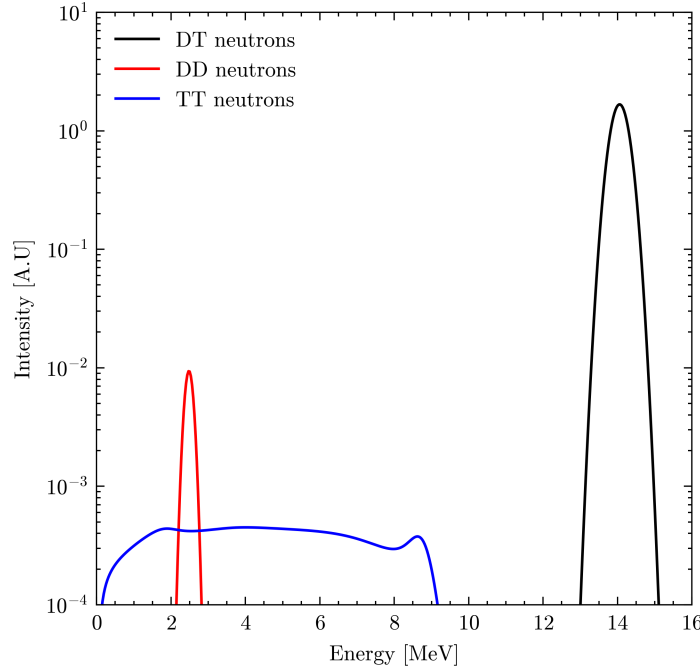


Figure 5: Neutron production spectra for each of the three reactions given by (3),(4),(5). Spectra are calculated using NeSST.

3.4 Streaming Term

The neutron transport equation, (12), employs an approximate form of the streaming term, $\frac{-v}{L}$. This approximation is that the flux through the surface of a computational cell is given by some characteristic loss length scale, equivalent to the average distance a neutron travels before it leaves that computational cell. This term serves as the coupling between the transport equations that describe each layer of the system.

Being an approximation, the value of L is difficult to give with certainty; the method used to determine L is described here. A 1D discrete ordinates neutron transport code, Minotaur, developed at Imperial College London has the ability to simulate a spatially resolved neutron flux [47]. This was used to calculate the flux through the spherical surfaces of a spherical shell for a homogeneous neutron source. This calculation was performed for varying thicknesses of spherical shells with varying densities of ions that serve to scatter the neutron flux. From this, a polynomial fitting function was obtained that describes the flux through the outer surface of the shell as a function of the shell's dimensions and density. A second polynomial fitting function was obtained to describe the flux through the inner surface. An evaluation of the validity of the approximation is given in section 4.1.3.

3.5 Target Doping Functionality

The target doping functionality implements the doping of ions into the capsule, replicating the capabilities of techniques such as VORCAN and ANDARIST at NIF. These techniques typically add the dopant to the inside of the ablator layer, but the dopant may become

mixed through the capsule due to hydrodynamic effects during the implosion process. This model makes no attempt to quantify this effect but, to recreate the various possible mixing scenarios, dopant ions may be added to any of the layers specified in the structure of the capsule.

The model has the ability to dope four ion species into the capsule. Dopant target ions are specified by a reaction name. For example ‘ $^{171}\text{Tm}(n,\text{G})$ ’ is used to represent the neutron capture by ^{171}Tm to form ^{172}Tm . In addition to the reaction, the location and number density of the dopant species must also be specified. Reaction cross-sections are taken from nuclear databases such as ENDF. A linear interpolation is performed such that the cross-section is evaluated for each energy bin, and is then added to the scattering matrix for simplicity of implementation.

The reaction cross-section probabilistically removes neutrons from the relevant capsule layer at each computational time-step, simulating the capture of neutrons by the target species. These neutrons are then added to a hypothetical additional system used for analysis of the spectrum of energies at which captures occur. This system serves only to collect ‘captured’ neutrons, and so is not described by any transport equation.

3.6 Construction of ODE system

For the purpose of this model, a doped ICF capsule is fully described by the capsule parameters and the dopant parameters. Capsule parameters consist of the number density, layer thickness and fraction by number density of each of the included ion species. These parameters must be specified for each of the layers in the capsule composition.

A system of coupled ordinary differential equations is constructed that describes a system composed of three parts:

1. The capsule consists of layers that mirror the construction of an ICF capsule. The innermost layer is where fusion reactions take place, and so it has a non-zero neutron source term in its neutron transport equation. All layers are described by a neutron transport equation, where the transport in the various layers is coupled by the flux between layers. Each layer has a flux leaving its surfaces, which determines the flux entering its adjacent layers. Using the target doping functionality, any of the capsule’s layers may be doped. Under the approximation that neutron velocity is far greater than typical fluid velocities, the capsule is assumed to be static, and so the dimensions of the layers are constant throughout the simulation.
2. The environment surrounding the capsule is a separate system. It is assumed to be a vacuum of infinite size. As there is no medium for neutrons to interact with, this layer is not described by a neutron transport equation. It receives neutrons from the outermost layer of the capsule, and serves only to accumulate neutrons over time.
3. There are four target layers that form an additional hypothetical system. These layers accumulate the spectrum of neutrons removed from the capsule system by target ions doped into the capsule composition. Similarly to the environment layer, these layers are not described by transport equations as these neutrons do not interact. The purpose of these layers is only to collect neutrons for analysis.

3.7 Interpretation of the Model

It is important to put the implementation of the various features outlined in the previous sections into context to understand their impact on the physical meaning of results so that they can be interpreted correctly.

The model calculates a time-dependent spectrum of the neutron flux for each layer of the capsule. This spectrum is a flux per unit energy (referred to here as neutron intensity), and so must be interpreted in the context of the energy binning employed. As many of the results presented in this work use logarithmic binning, there is potential to misinterpret results. As such, neutron spectra are typically integrated over energy bin width to present a total neutron flux in each energy bin. Similarly, the spectrum of neutron capture events is a number of captures per unit energy. Any plots showing this are integrated over energy bin widths to present the total number of captures in each energy bin. Where this is done, the units of the relevant axes are stated explicitly.

4 Results

4.1 Model Verification

4.1.1 Comparison to Analytic Solution

To test the scattering functionality of the model, the elastic scattering of a unit monoenergetic neutron source by some uniform total and differential cross-section in an infinite volume was considered, and compared to the analytic solution for this case. This comparison is useful to verify that the construction of the scattering matrices has implemented scattering as expected.

The analytic solution was obtained by first parametrising in terms of $\tau = n\sigma vt$. The streaming term was removed since no flux of neutrons leaves a system of infinite size. This gives a transport equation of the form

$$\frac{d\phi}{d\tau} = -\phi + \frac{1}{\sigma} \int \frac{d\sigma}{dE} \phi dE \quad (17)$$

where $\phi = \sum_{s=0}^{\infty} \phi_s$ allows for this to be written in terms of the s^{th} scattered component, which is given by

$$\frac{d\phi_s}{d\tau} = -\phi_s + \frac{1}{\sigma} \int \frac{d\sigma}{dE} \phi_{s-1} dE. \quad (18)$$

Multiplying by e^τ and recognising that $e^\tau \frac{d\phi_s}{d\tau} + e^\tau \phi_s = \frac{d}{d\tau} [e^\tau \phi_s]$ yields the solution given by

$$\phi_s = \frac{1}{\sigma} \int \frac{d\sigma}{dE} \phi_{s-1} dE. \quad (19)$$

The numerical solution was found by matrix multiplication of a scattering matrix for a hypothetical scatterer with a flat, total cross-section of unit magnitude with a monoenergetic unit source. A total cross-section of magnitude unity means that every neutron must scatter, so performing an iterative calculation given by

$$\phi_0 = \delta(E - E_0), \quad \phi_{s+1} = \phi_s + \frac{d\phi}{dt}|_{\phi=\phi_s} \quad (20)$$

where $\frac{d\phi}{dt}|_{\phi=\phi_s}$ is given by

$$\frac{d\phi}{dt}|_{\phi=\phi_s} = nv[-\sigma + \sum_{E_n} \frac{d\sigma}{dE_n} \Delta E_n] \phi_s \quad (21)$$

yields the s^{th} scattered component to the neutron spectrum. The first four components are shown in Fig.6, where it is clearly seen that the numerical solution matches the analytic, verifying that the scattering matrices correctly implement scattering mechanics.

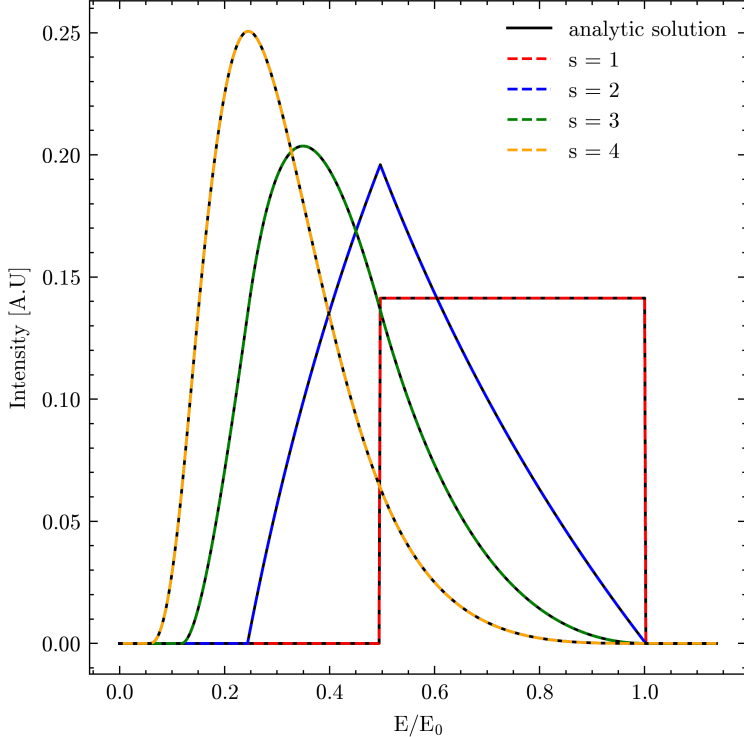


Figure 6: Comparison of analytic solution (19), to numerical solutions (20),(21), for scattering of a monoenergetic neutron source by a uniform scatterer.

4.1.2 High-Energy Behaviour

Comparison to the predictions of a more complex model in the high-energy regime was used to verify that the behaviour for energies above 1MeV is as expected. The left plot in Fig.7 shows a neutron spectrum calculated by a discrete ordinates neutron transport code, Minotaur [47]. Minotaur discretises space into 64 angular bins and 400 energy bins. The increased angular resolution of Minotaur over the model developed here makes this model suitable for post-processing hydrodynamics simulations. There are two recognisable features of this spectrum that the model developed is expected to replicate.

The first of these is the primary neutron peaks. These can be seen at 2.45MeV for DD neutrons and 14MeV for DT neutrons. Through comparison to the plot on the right of Fig.7, it is seen that the relative heights of these peaks is similar, showing that the neutron source term correctly simulates the neutron produced in fusion reactions. Additionally, comparison of the heights of the peaks in relation to the scattered components of the spectra shows that scattering plays the correct contribution to the overall shape of the spectrum.

Another validation of the scattering implementation comes from examining the backscatter edges. These can be seen at around 2MeV and 4MeV , on either side of the DD peak, and are the energy that 14MeV DT neutrons are scattered down to when they scatter 180° off either a deuterium or tritium ion. Since the angular trajectory of neutrons was integrated out (as seen in (10)), this shows that the differential cross-section (as opposed to the double differential cross-section) correctly implements scattering mechanics.

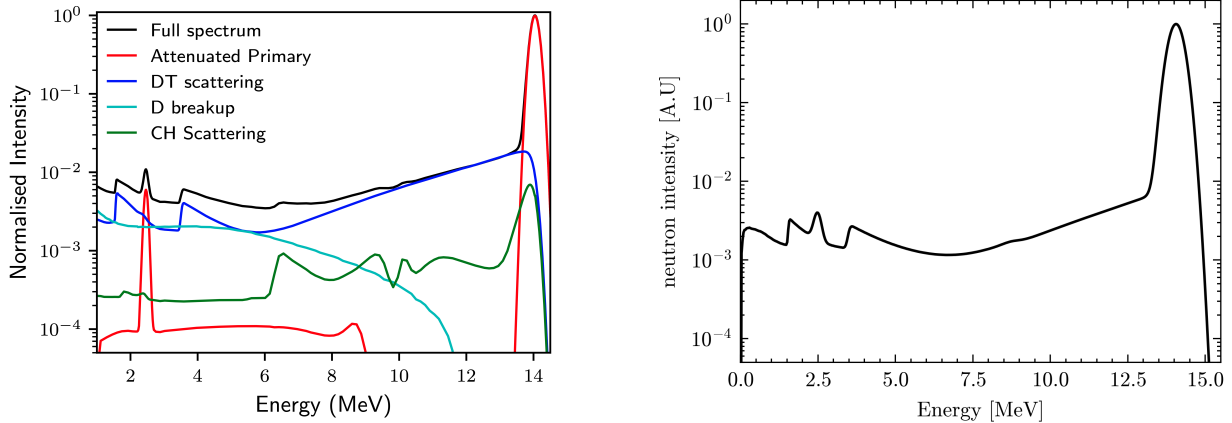


Figure 7: (Left) Neutron Spectrum modelled using Minotaur, a discrete ordinates transport code used to post-process hydrodynamics simulations [41]. The full spectrum is of interest as a comparison to the predictions of the developed model. Taken from [48]. (Right) Neutron spectrum outside a typical cryogenic ignition capsule.

4.1.3 Streaming-Term Behaviour

Presented here is a numerical validation of the approximation applied to the streaming term as was derived in section 2.1.2. The plot in Fig.8 shows the loss length scale, L , in red. The black trace shows L as calculated from a spatially resolved neutron flux by a discrete ordinates neutron transport code, Minotaur [47]. It can be seen from the plot that the steady state, meaning constant flux through the spherical surface that corresponds to the surface of the computational cell, is reached at around $15ps$. At this point, the constant loss length scale becomes a good approximation. This tells us that the approximate form of the streaming term can resolve a time-varying neutron source that varies over longer timescales than $15ps$. A typical neutron source used in the model is a Gaussian with $\sigma \approx 25ps$, so the use of a constant loss length scale is an appropriate approximation when put in the context of the use-case of the model.

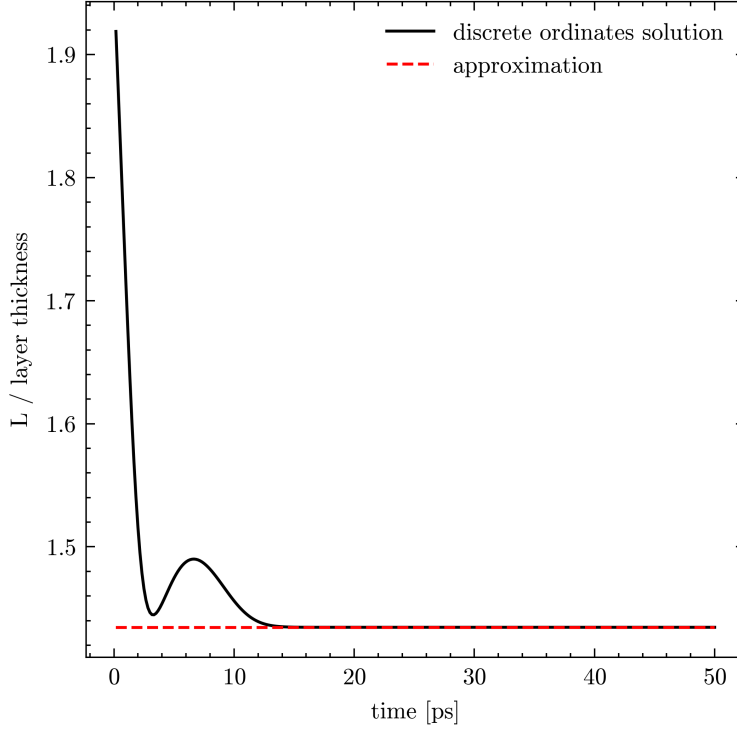


Figure 8: Plot of the ratio of the loss length scale, L , to layer thickness as a function of time. Black trace is calculated by a discrete ordinates transport code, Minotaur [47], for a constant monoenergetic neutron source inside a spherical shell.

4.2 Investigation Results

4.2.1 Capsule Design and Fusion Fuel Investigation

In this section, the core functionality of the model is introduced through a short investigation into the neutron spectra for the different fusion fuels and capsule designs described in section 1.4.1. The table below shows the relevant parameters for a typical cryogenic ignition capsule and PDXP capsule.

Capsule	Layer Number	Layer Name	Layer Number Density [cm ⁻³]	Layer Width [μm]
Cryogenic Ignition Capsule	1	Hotspot	10^{30}	35
	2	Fuel Shell	10^{32}	10
	3	Carbon Ablator	10^{32}	10
PDXP Capsule	1	Fuel Region	10^{30}	450
	2	Carbon Ablator	10^{32}	50

Table I: Capsule parameters used for the investigation in section 4.2.1. Layer densities and widths are typical values at the time where fusion reactions begin to occur.

The graph in Fig.9 shows the predicted spectrum outside the capsule given as neutron flux per unit energy integrated over energy bin width. There is a larger low-energy flux in the cryogenic ignition capsule, indicating that the higher density of this capsule as compared to

the PDXP capsule is an important factor governing the amount of neutron scattering that occurs.

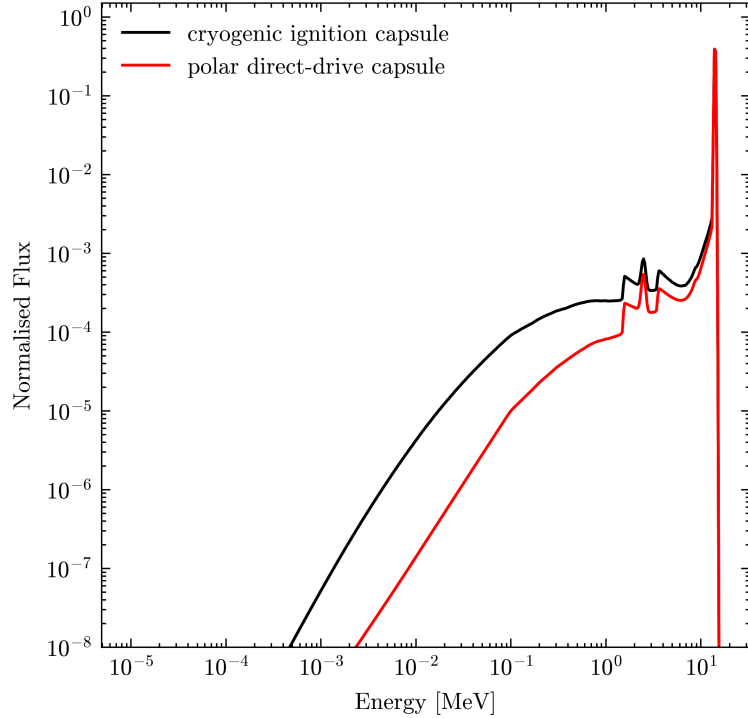


Figure 9: Comparison of a typical cryogenic ignition target fielded at NIF to a PDXP target. Both capsules contain DT fuel.

The graphs in Fig.10 show a comparison of the spectra outside the capsule for the capsule designs for either DT or deuterium fuel. Results are presented as neutron flux integrated over energy bin widths. Of particular interest is the comparison of fluxes in a PDXP capsule, seen on the right-hand side of Fig.10. The fact that the red trace falls off more quickly than the black signals that deuterium fuel results in a more monoenergetic neutron source than DT fuel. This effect is compounded because there is no 14MeV DT neutron peak.

4.2.2 Investigation into Neutron Moderation

The measurement of a neutron capture cross-section using ICF technology can inherently only be performed at a single energy in each experiment. To maximise the applicability of measurements to astrophysical scenarios, it is preferable that this energy is similar to those at which nucleosynthesis occurs in stars ($\sim 30\text{keV}$). Experimentally, the optimal scenario is that the spectrum of energies at which neutron capture takes place is concentrated over a small energy range. To investigate the extent to which these criteria are achievable, a study into neutron moderation was performed.

Moderation of neutron flux can be achieved through modification of the capsule composition to include ion species which are expected to be good moderators of neutron flux. By considering classical scattering, it can be seen that hydrogen, an ion with the same mass as a neutron, is expected to be the most effective moderator. There is precedent for using

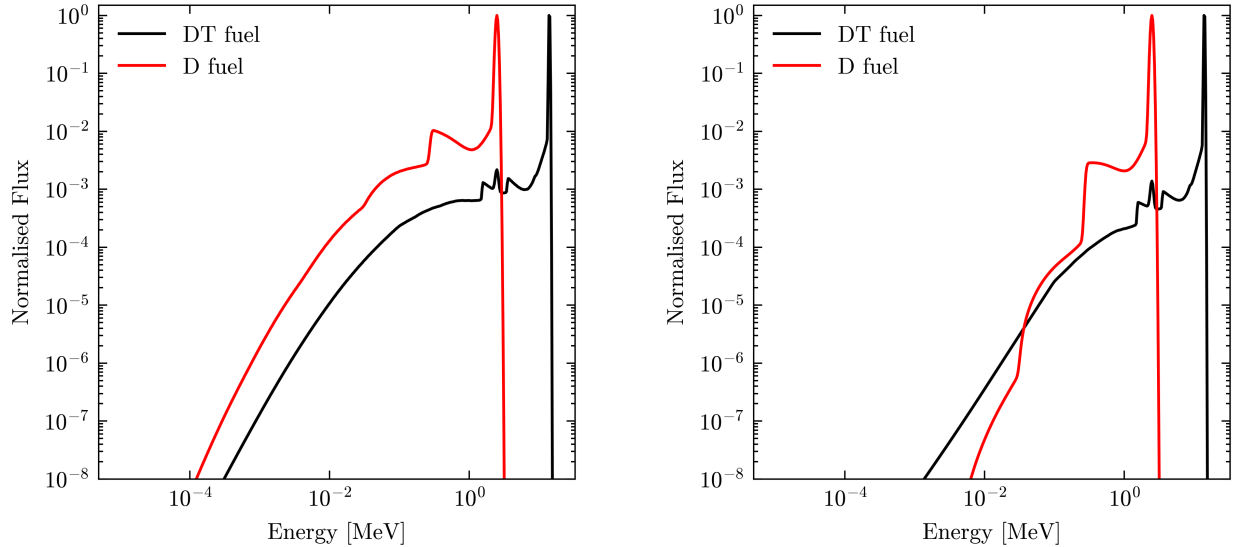


Figure 10: (Left) Comparison of DT fuel with deuterium fuel in a cryogenic ignition capsule. (Right) Comparison of DT fuel with deuterium fuel in a PDXP capsule. The red trace is lower than the black trace at low energies, showing that deuterium fuel results in a more monoenergetic neutron source.

a non-50:50 mixture of DT fuel, instead adding a significant amount of hydrogen to the composition [49], [50], [51]. Early in the National Ignition Campaign at NIF [52], Hydrogen was added in large amounts to ‘dud’ an implosion, drastically reducing its yield to protect diagnostics equipment. Whilst the effect of different fuel compositions is an interesting area of research [53], consideration of the detrimental effect of a sub-optimal fuel mixture is beyond the scope of this model. The decrease in the mass of fusion fuel is accounted for in the neutron yield, but there is no attempt made to quantify hydrodynamic effects of altering the fuel composition.

PDXP capsules are the proposed platform for performing cross-section measurements, and results presented here use this design. The plot in Fig.11 shows that moderation of deuterium fuel is more effective at enhancing neutron flux at stellar relevant energies than DT fuel. This is because all neutrons are produced at 2.45MeV , and so require fewer interactions to be moderated to below 100keV when compared to 14MeV DT neutrons. Thus the aim of this investigation was to find the optimum position and amount of hydrogen to add to a deuterium-filled PDXP capsule to maximise the number of neutron capture events at the energy at which the cross-section of neutron capture is to be measured.

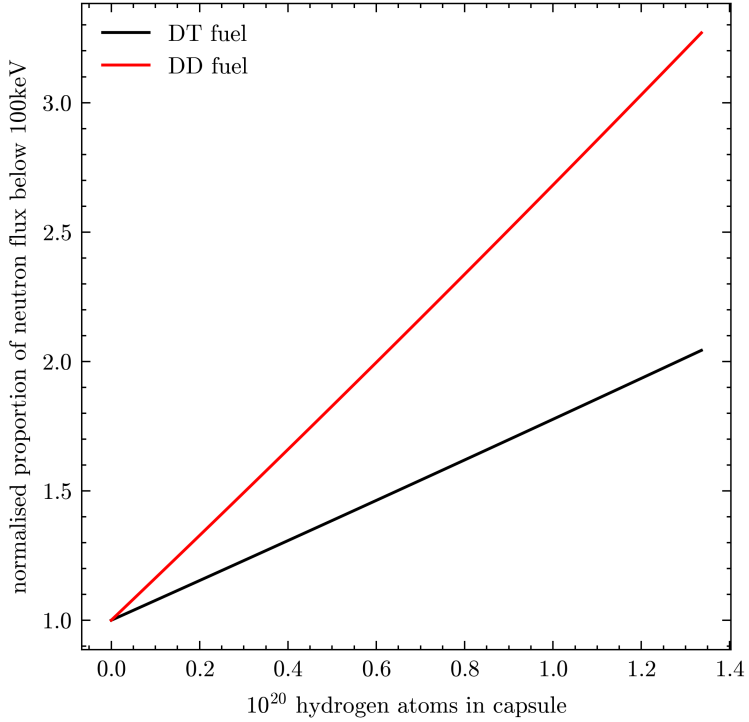


Figure 11: Plot of the increase in the proportion of total neutron flux below 100keV as hydrogen is added to the capsule. Moderating deuterium fuel is more effective at increasing the proportion of low energy flux.

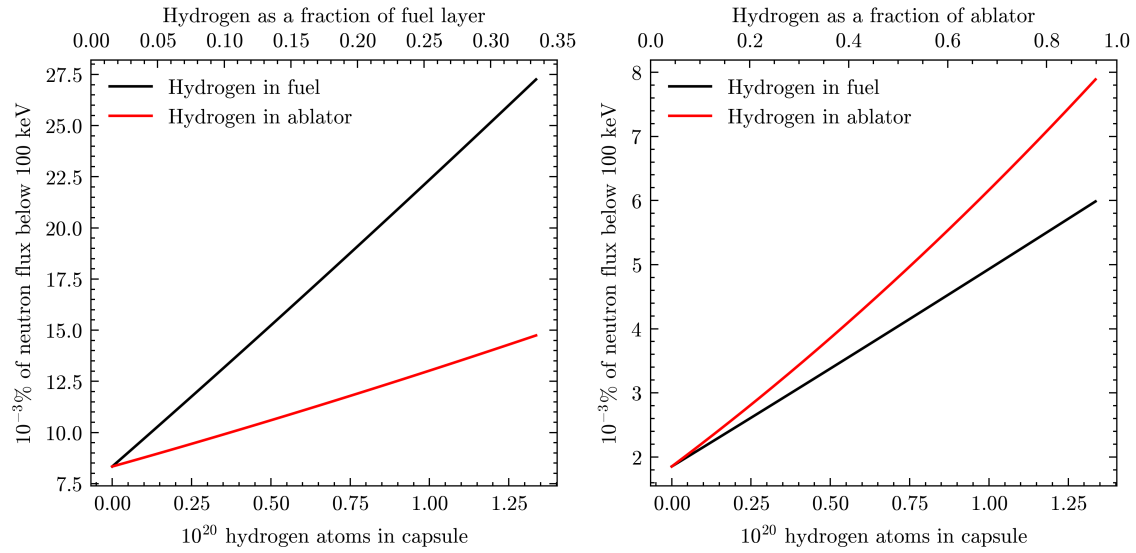


Figure 12: (left) Plot of the percentage of neutron flux below 100keV in the fuel layer of a PDXP capsule as hydrogen is added. (right) Plot of the percentage of neutron flux below 100keV in the ablator of a PDXP capsule as hydrogen is added.

The plots in Fig.12 compare the increase in low energy (defined here as below 100keV)

neutron flux in each of the layers of the capsule for the same amount of hydrogen added into either the fuel layer or ablator. It can be seen from these plots that the flux in each layer is increased most effectively by adding hydrogen to that layer.

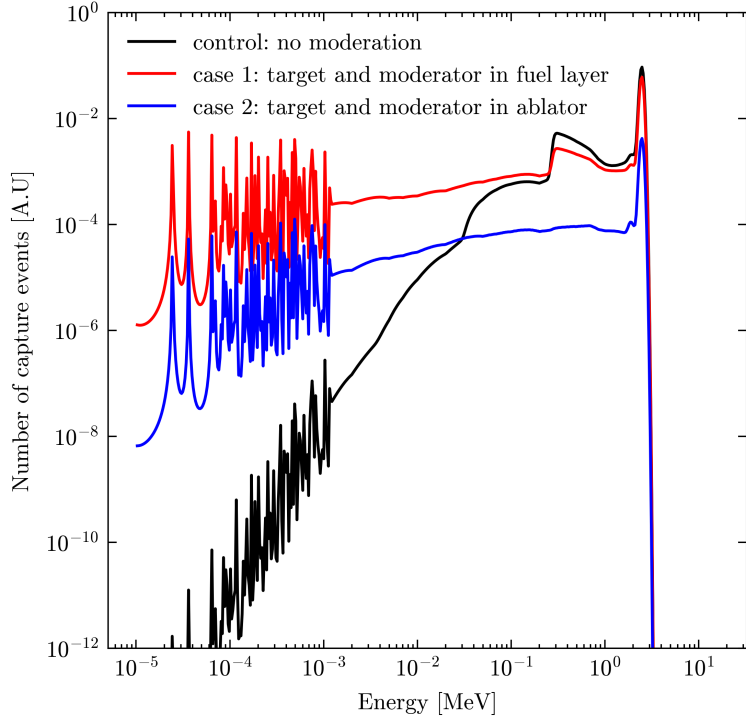


Figure 13: Plot of the spectrum of neutron captures by ^{171}Tm for moderated and unmoderated PDXP capsules. The spectrum of captures has been integrated over bin widths, giving the total number of captures in each energy bin.

The plot in Fig.13 shows a comparison of the number of neutron captures by ^{171}Tm for three scenarios. The black trace gives the captures occurring in an unmoderated capsule. The red and blue traces give the number of captures in a capsule moderated by adding 1.3×10^{20} hydrogen atoms to the optimum location for moderation for each of the cases as was learned from Fig.12. It can be seen by comparing the black to coloured traces that moderation by hydrogen has successfully enhanced the low-energy neutron flux such that more captures take place at these energies. However, since a cross-section measurement can inherently only be performed at a single energy, the process of neutron moderation has introduced additional uncertainty as to the energy at which the measurement has taken place.

4.2.3 Investigation of Experimental Procedure for Cross-Section Measurements

Calculating a neutron capture cross-section from experiment requires two pieces of data: the number of neutron capture events and the flux experienced by the target ion species (referred to as the test species). As was described in section 1.4.2, methods for counting the number of capture events are well-established. A simple way to directly measure the flux experienced by the test species is to dope an additional target species (referred to as the monitor species)

with a known neutron capture cross-section into the capsule. Based on the number of neutron captures that take place in the monitor species, the neutron flux is calculated. It can be seen from the plot in Fig.14 that the neutron flux in different layers of the capsule can vary by around a factor of 5 at the point of maximum neutron flux, implying that the flux experienced by the monitor species may not be representative of the flux observed by the test species if they are found in different regions of the capsule. This means that if the different target species are to mix differently through the capsule during the implosion process, it can be expected that they experience a different neutron flux. This would result in a different number of neutron captures by the two species, leading to a prediction of a different neutron flux by the monitor species than was experienced by the test species. This would introduce additional uncertainty into the cross-section measurement. Since the validity of the assumption that the test and monitor species observe the same neutron flux is central to the precision of a cross-section measurement, an investigation into target mixing was performed.

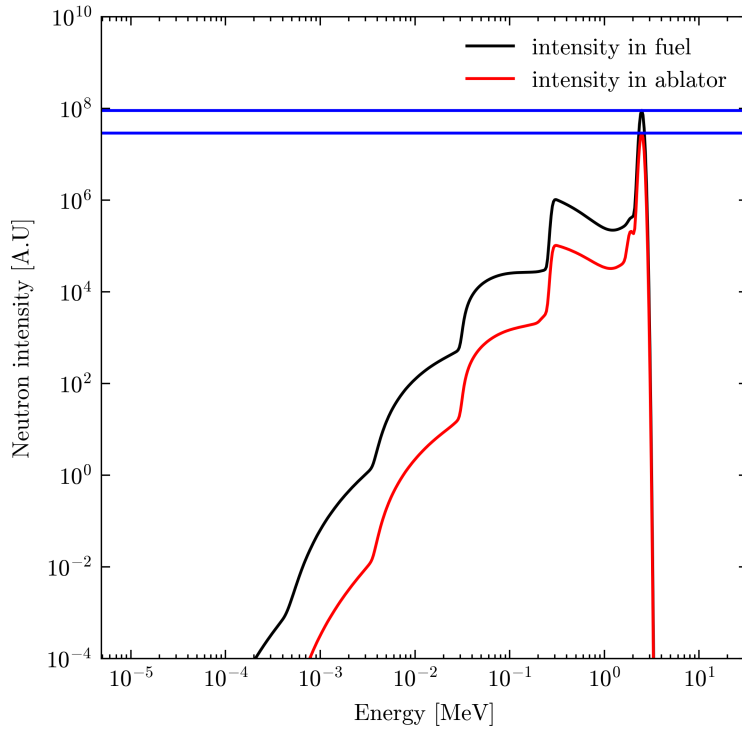


Figure 14: Plot of neutron intensity (flux per unit energy in each energy bin) in the fuel layer and ablator of a deuterium-filled PDXP capsule. The blue lines indicate a difference of around a factor of 5 in neutron fluxes at the energy at which neutron intensity is a maximum.

The target doping functionality, as described in section 3.5, can be used to dope target ions into a specific layer of the capsule composition. Partitioning of a region of the capsule so that it is represented by two ‘layers’ in the model that have the same properties allows for precise control over the extent of the mixing of a target species. These partitions will be referred to as ‘artificial partitions’. Where an artificial partition is used in the fusioning fuel layer, the neutron source term is distributed on both sides of the partition by the ratio of

the volumes of each region.

For this investigation, two separate populations of ^{171}Tm ions were added into the capsule to serve as the monitor and test species. The ratio of the number of captures between the two populations was found as the extent to which the species were mixed throughout a deuterium-filled PDXP capsule is varied. A diagram illustrating this is shown on the left-hand side of Fig.15, and is described here.

The doping of the target species into the ablator and subsequent mixing through the response to shocks was simulated for the two ion species as follows:

1. The poorly-mixed target was doped only into the ablator. The mixing of the poorly-mixed species was kept constant throughout the experiment, simulating an ion species that responds poorly to shocks passing through the capsule.
2. The well-mixed target was doped into the ablator and the outer portion of the partitioned fuel region. The position of the partition could then be used to control the thickness of the spherical shell that contained the well-mixed target species, simulating an ion species that responds positively to shocks and becomes mixed throughout some portion of the capsule.

By examining the graph on the right-hand side of Fig.15, it was predicted that a discrepancy of around 100% is expected to be observed in the case of one ion species being almost homogeneously mixed throughout the capsule, and another species remaining at the edge of the capsule. This means that if the extent of mixing of the two ion species is completely unknown, then a significant error may be introduced into the measurement. The shape of the black trace will be dissected into its contributions to justify the shape, which are shown in the inset graph on the right-hand side of Fig.15.

The blue trace shows the number of captures in the well-mixed species, which follows the expected trend. The number of captures increases rapidly at first and then plateaus, just as the volume of a spherical shell increases when increased in thickness radially inwards. This shows that target ions present in the fuel region are more likely to capture neutrons. The structure on top of this trend is likely an artefact of the model, due to the increment of the position of the artificial partition altering the transport solution, where it is expected to remain constant throughout the experiment.

The red trace shows the number of neutron captures in the poorly-mixed species, which does not follow the expected trend. Since the extent to which the poorly-mixed species is kept constant throughout the experiment (it is always mixed homogeneously throughout the ablator), the number of captures in this species is expected to be constant throughout the experiment, or to possibly decrease slightly due to a shielding effect from the well-mixed species. This unexpected behaviour is attributed to an artefact of the model, with the movement of the artificial partition altering the transport solution. Assuming that a constant number of captures in the poorly-mixed species was expected to be observed, the uncertainty introduced by artefacts in the model can be quantified to be around 25%. This uncertainty is small enough that the conclusions drawn from these results are unchanged, and have significant implications for experimental methods used for cross-section measurements at NIF.

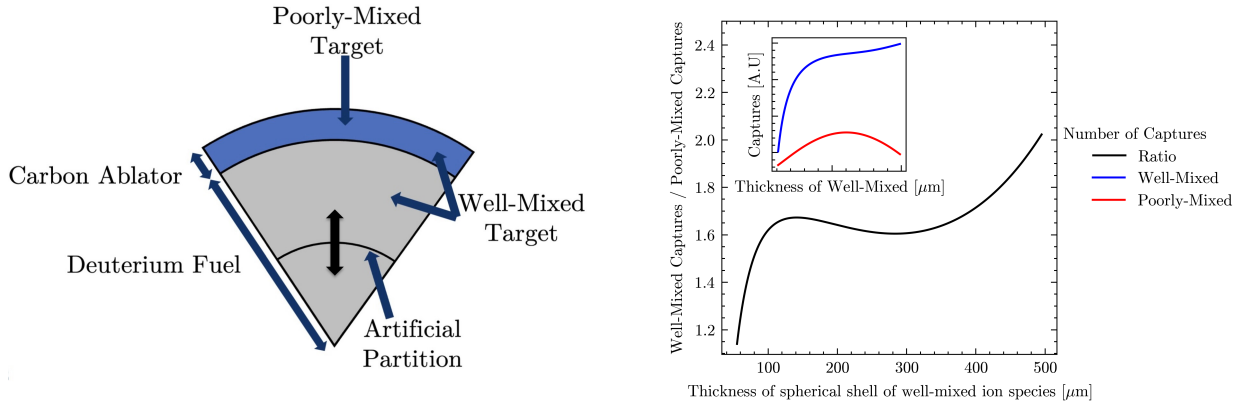


Figure 15: (Left) Schematic of the target mixing experiment. The position of the artificial partition is moved radially inwards to control the extent to which the well-mixed target is mixed throughout the capsule. (Right) Plot of the ratio of captures by a well-mixed species and a poorly-mixed species. The inset graph shows the number of captures for each species.

5 Discussion

5.1 Discussion of Results

5.1.1 Capsule Design and Fusion Fuel Investigation

The investigation into capsule and fuel types gave two main results. Firstly, it was shown that, of the two main capsule types, the ignition focused capsule had the broader neutron spectrum, meaning that there was a greater neutron flux at low energies compared to the PDXP capsule. This is because the higher areal density achieved during the implosion of an ignition capsule resulted in more scattering events, and so additional moderation of the neutron flux in comparison to the larger, but less dense PDXP capsule design. Results in this area have limited application to nucleosynthesis experiments, but were presented as an introduction to the abilities of the model. Despite this, some key results are quoted as motivation for design choices in later experiments into neutron moderation and target mixing. The main result from this investigation is that a deuterium-filled PDXP capsule is expected to produce a narrow neutron spectrum, making it a viable neutron source for successful cross-section measurements. Planned experiments for the measurement of neutron capture cross-sections have proposed to use PDXP capsules for their hydrodynamic stability and operation below the NIF optics damage threshold, so this result serves as further motivation for their applicability to this type of experiment.

5.1.2 Neutron Moderation Investigation

The investigation into neutron moderation was performed for a PDXP capsule, with varying amounts of hydrogen added to the capsule composition with the motivation that hydrogen was expected to be an effective moderator of neutron flux. The aim of this investigation was to find the optimum position and location to add hydrogen to the capsule to maximise the

number of neutron capture events that occur at the energy at which the neutron capture cross-section of some s-process relevant element is to be measured. Based on the idea that some target species would be doped into the inner surface of the ablator by a technique such as VORCAN or ANDARIST at NIF, and that the response of these heavy ions to shocks is relatively unknown, the aim was to present results for the moderation of neutron flux in each of the layers of a PDXP capsule. As such, an experiment where some number of hydrogen atoms was doped into either the fuel region or the ablator of a PDXP capsule was simulated using the transport model developed for this work. The increase in the proportion of the total neutron flux that was below a threshold of 100keV was presented. This energy threshold was chosen as it is a rough boundary between ICF-relevant and astrophysical-relevant energies. It was found that the addition of hydrogen into the capsule composition was able to successfully enhance the low energy neutron flux through increased moderation of the primary ICF neutrons. For neutrons to be scattered down to such energies, they must undergo multiple scattering events, highlighting the success of our model in this respect.

In addition to this, the target doping functionality of the model allowed for analysis of the spectrum of energies at which neutron capture events took place. A comparison of the number of captures in ^{171}Tm for an unmoderated deuterium-filled PDXP capsule was compared to two different moderated cases. These two cases were derived from the moderation results, using the optimum position of hydrogen to boost the low energy flux in each of the two regions of the capsule. Comparison to the unmoderated case verified that the moderation had successfully enhanced the low energy flux, as there were significantly more captures occurring at stellar-relevant energies. However, it was also found that moderation by hydrogen was not effective enough to be a viable method of performing neutron capture cross-section measurements at stellar-relevant energies. This is due to the fact that a cross-section measurement can inherently only be performed at a single energy in any given experiment. Since it was shown that the low energy flux enhancement served to flatten out the spectrum at which captures occurred, this would introduce more uncertainty as to the energy at which the measurement was performed, and it can be concluded that moderation by hydrogen is not effective enough for use in this type of experiment.

Despite this conclusion, neutron moderation in ICF experiments has been shown to have potential for use in the future. Whilst it has been shown that the amount of hydrogen that can feasibly be added to current capsule designs is arguably detrimental to the success of a cross-section measurement, it was shown that hydrogen is an effective moderator of neutron flux. If future developments lead to higher achievable areal densities, moderation by hydrogen could conceivably be more effective. Alternatively, it would be possible to construct a scattering medium outside of the capsule to moderate the neutron flux emerging from a capsule. This would sacrifice a key benefit of the use of ICF technology, in that the target nuclei would need to be located outside of the capsule, and could not take advantage of the HED environment to populate excited nuclear states. There are many engineering challenges facing either of these potential solutions, and they are areas of ongoing research [54], [55].

5.1.3 Target Mixing Investigation

The primary goal of this work was to investigate the viability of neutron moderation for stellar nucleosynthesis experiments. However, the flexibility of the model in terms of capsule

structure and composition, combined with its computational simplicity meant that the model could be developed beyond its original intended application to investigate the robustness of the intended experimental method for measuring neutron capture cross-sections using ICF technology.

As these experimental methods propose to dope multiple radiochemical detectors into the capsule, an investigation into their mixing through a capsule was performed. A species with a known cross-section is proposed to be used as a direct experimental observation of the neutron flux experienced by the test species.

PDXP capsules are primarily heated through the application of shocks rather than through compression. The effect this has on the mixing of ions through the capsule is beyond the scope of this work, but it was predicted by the model that if they are to mix differently throughout the capsule, then they should experience a different neutron flux. A difference in the neutron flux experienced by the target species would result in a different number of captures. This in turn would impact the prediction of the neutron flux observed by the test ion species as predicted by the monitor ion species, introducing uncertainty into any calculation of a neutron capture cross-section. To investigate the implications of unequal mixing, an experiment where the effect of varied target mixing on the difference in the number of captures between two ion species was performed.

Whilst it is acknowledged that results were impacted by artefacts arising from the spatial averaging applied to the transport equation and by the introduction of an artificial partition into the fuel region, it was concluded that the key findings of this investigation held true. It was concluded that, if target mixing was determined to be poorly understood, the worst case scenario would present a 100% error in the flux predicted by the monitor test species. This uncertainty would propagate into the calculation of a neutron capture cross-section introducing significant error. Therefore, it can be concluded that the response of heavy ions to shocks must be better understood before this type of experiment can be fielded experimentally.

5.1.4 Proposal of Experimental Design

Based on the findings of this work, an experimental design for the measurement of a neutron capture cross-section at NIF is proposed. Firstly, from the conclusion that neutron moderation is not effective, there is motivation to use a combination of capsule design and fusion fuel that results in the most monoenergetic neutron flux, regardless of whether or not the cross-section measurement is performed at a stellar-relevant energy. It has been shown that a deuterium-filled PDXP capsule results in a narrow spectrum of neutron energies around 2.45MeV since the low areal densities achieved by this capsule design result in little moderation of the neutron flux. Secondly, following on from the conclusion that the mixing of target species throughout the capsule must be better understood, research in this area must be performed before such an experiment can be fielded. In addition to this, doping additional monitor species into the capsule presents an opportunity for multiple predictions of the neutron flux experienced by the test species. Having multiple data points for the neutron flux would mean that unequal mixing of the various target species could easily be recognised. This would allow for the implementation of an upper-bound on the acceptable level of uncertainty that may be introduced by unequal target mixing through a statistical

analysis of these data points.

5.2 Limitations of the Model

The criteria for the model were set out in section 1.5. The central aim of the model was to predict the ICF neutron spectrum at stellar-relevant energies. Since ICF neutrons are produced with energies on the *MeV*-scale, neutrons must undergo multiple scattering events to be moderated to such energies. As a result, a strong importance was placed on the implementation of neutron scattering, and it was important that this was done in such a way that there would be no upper bound on the possible number of scattering events per neutron. Since the model was also developed with computational simplicity as a priority, there was necessarily a compromise to be struck between the resolution of other aspects of results. A clear example of this was seen in the removal of spatial resolution through the application of spatial averaging, and the removal of the dependence on the angular trajectory of neutrons. The simplifications and approximations applied necessarily introduced a limit on the complexity of the predictions that the model is capable of.

The main approximation of the model is the approximate form of the streaming term. As is shown in section 4.1.3, a constant loss length scale is a good approximation for the case where the neutron source evolves more slowly than the time taken to reach a constant flux through the surface of a layer. With the values of the loss length-scale being informed by a spatially-resolved transport model, this shows that to achieve a considerably greater accuracy than this would require a spatially resolved model, and development of the model in this respect is deemed beyond its original scope.

A second approximation that limits predictions is that of a static capsule. This approximation was applied under the assumption that neutron velocities are far greater than typical implosion velocities, and so a neutron ‘sees’ a static capsule. With typical implosion velocities being around 300km s^{-1} [56], this approximation holds for high energy neutrons ($\sim 10\text{MeV}$ neutrons have velocities $\sim 50,000\text{km s}^{-1}$). As such, this is a common approximation applied in ICF neutron transport models. However, with this model extending the spectrum down to around 10eV , this approximation begins to break down. A 10eV neutron has a velocity of around 50km s^{-1} . This is lower than the implosion velocity, and so the neutron passes through an evolving capsule. Including time-dependence of the size and properties of the capsule is a possible extension to this work, but it is important to consider the compromise that has been struck between predictive power and computational complexity.

6 Conclusions

A reduced-dimension neutron transport code for modelling the ICF neutron spectrum was developed. The central focus of the model was to extend knowledge of the neutron spectrum to below 1MeV to astrophysical-relevant energies to enable investigations into the application of ICF technology to nucleosynthesis experiments, in particular measurements of neutron capture cross-sections relevant to the slow neutron capture process. As such, importance was placed on the implementation of neutron scattering and energy resolution, which enabled investigations into neutron moderation and its application to cross-section measurements. It was found that, in its current capacity, neutron moderation through modification of the capsule fuel composition to include hydrogen is able to effectively enhance low energy neutron flux. However, this came at the expense of the monoenergeticity of the neutron spectrum, introducing additional uncertainty into any cross-section measurement. An additional investigation into the experimental procedure for such measurements found that a deeper understanding of the mixing of heavy ions through the capsule during the implosion process is critical to the success of a cross-section measurement.

6.1 Future Work

As the results presented in this work have served as preliminary investigations into the experimental procedure for cross-section measurements using ICF technology, there is motivation to pursue directions of additional research in various areas.

Firstly, lifting the approximation of a static capsule is a compelling direction for further model development. Implementing time-varying capsule properties that could be informed by simple 1D hydrodynamics simulations would improve the accuracy of results at lower energies.

Secondly, the investigation into neutron moderation showed that hydrogen was ineffective for use as a moderator in cross-section measurement experiments. The use of hydrogen was motivated by classical arguments, and the availability of total and differential cross-section data simplified its inclusion in the model. Further investigation into alternative materials such as beryllium or boron would enable a more comprehensive stance on the viability of neutron moderation inside an ICF capsule.

Finally, the investigation into target mixing motivates additional research into the mixing of heavy ions through a capsule due to shocks. It was shown that increased understanding is critical before a measurement can be performed. Development of our understanding of the possible mixing scenarios could be used to inform a more detailed investigation using the model, as physically justified mixing scenarios would enable a quantitative analysis of uncertainties.

7 Appendix

7.1 Access to Code

A link is provided to a GitHub repository with the code for the neutron transport model developed for this work: 'https://github.com/brynlloyd1/Msci_Neutron_Transport_Model'.

References

- [1] Post RF. Controlled Fusion Research—An Application of the Physics of High Temperature Plasmas. *Reviews of Modern Physics*. 1956 Jul;28(3):338-62. Available from: <https://link.aps.org/doi/10.1103/RevModPhys.28.338>.
- [2] Atzeni S, Meyer-ter Vehn J. *The Physics of Inertial Fusion*. Oxford University Press; 2004. Available from: <https://academic.oup.com/book/27812>.
- [3] Ongena J, Koch R, Wolf R, Zohm H. Magnetic-confinement fusion. *Nature Physics*. 2016 May;12(5):398-410. Available from: <https://www.nature.com/articles/nphys3745>.
- [4] Braams CM, Stott PE. Nuclear Fusion: half a century of magnetic confinement research. *Plasma Physics and Controlled Fusion*. 2002 Aug;44(8):1767-7. Available from: <https://iopscience.iop.org/article/10.1088/0741-3335/44/8/701>.
- [5] Chadwick MB, Obložinský P, Herman M, Greene NM, McKnight RD, Smith DL, et al. ENDF/B-VII.0: Next Generation Evaluated Nuclear Data Library for Nuclear Science and Technology. *Nuclear Data Sheets*. 2006 Dec;107(12):2931-3060. Available from: <https://linkinghub.elsevier.com/retrieve/pii/S0090375206000871>.
- [6] Lawson JD. Some Criteria for a Power Producing Thermonuclear Reactor. *Proceedings of the Physical Society Section B*. 1957 Jan;70(1):6-10. Available from: <https://iopscience.iop.org/article/10.1088/0370-1301/70/1/303>.
- [7] Fraley GS, Linnebur EJ, Mason RJ, Morse RL. Thermonuclear burn characteristics of compressed deuterium-tritium microspheres. *The Physics of Fluids*. 1974 Feb;17(2):474-89. Available from: <https://pubs.aip.org/pfl/article/17/2/474/894718/Thermonuclear-burn-characteristics-of-compressed>.
- [8] Moses EI, Atherton J, Lagin L, Larson D, Keane C, MacGowan B, et al. The National Ignition Facility: Transition to a User Facility. *Journal of Physics: Conference Series*. 2016 Mar;688:012073. Available from: <https://iopscience.iop.org/article/10.1088/1742-6596/688/1/012073>.
- [9] Zylstra AB, Hurricane OA, Callahan DA, Kritch AL, Ralph JE, Robey HF, et al. Burning plasma achieved in inertial fusion. *Nature*. 2022 Jan;601(7894):542-8. Available from: <https://www.nature.com/articles/s41586-021-04281-w>.
- [10] Abu-Shwareb H, Acree R, Adams P, Adams J, Addis B, Aden R, et al. Lawson Criterion for Ignition Exceeded in an Inertial Fusion Experiment. *Physical Review Letters*. 2022 Aug;129(7):075001. Available from: <https://link.aps.org/doi/10.1103/PhysRevLett.129.075001>.
- [11] Appelbe B, Chittenden J. The production spectrum in fusion plasmas. *Plasma Physics and Controlled Fusion*. 2011 Apr;53(4):045002. Available from: <https://iopscience.iop.org/article/10.1088/0741-3335/53/4/045002>.
- [12] Bell G, Glasstone S. *Nuclear Reactor Theory*. US Atomic Energy Commision; 1970.

- [13] MCNP® Website;. Available from: <https://mcnp.lanl.gov/>.
- [14] Crilly AJ, Appelbe BD, Mannion OM, Forrest CJ, Knauer JP, Schlossberg DJ, et al. Neutron backscatter edges as a diagnostic of burn propagation. *Physics of Plasmas*. 2022 Jun;29(6):062707. Available from: <https://pubs.aip.org/pop/article/29/6/062707/2847948/Neutron-backscatter-edges-as-a-diagnostic-of-burn>.
- [15] Crilly AJ, Appelbe BD, Mannion OM, Forrest CJ, GopalaSwamy V, Walsh CA, et al. Neutron backscatter edge: A measure of the hydrodynamic properties of the dense DT fuel at stagnation in ICF experiments. *Physics of Plasmas*. 2020 Jan;27(1):012701. Available from: <https://pubs.aip.org/pop/article/27/1/012701/262967/Neutron-backscatter-edge-A-measure-of-the>.
- [16] Chittenden JP, Appelbe BD, Manke F, McGlinchey K, Niasse NPL. Signatures of asymmetry in neutron spectra and images predicted by three-dimensional radiation hydrodynamics simulations of indirect drive implosions. *Physics of Plasmas*. 2016 May;23(5):052708. Available from: <https://pubs.aip.org/pop/article/23/5/052708/958921/Signatures-of-asymmetry-in-neutron-spectra-and>.
- [17] Burbidge EM, Burbidge GR, Fowler WA, Hoyle F. Synthesis of the Elements in Stars. *Reviews of Modern Physics*. 1957 Oct;29(4):547-650. Available from: <https://link.aps.org/doi/10.1103/RevModPhys.29.547>.
- [18] Cameron AGW. Nuclear Reactions in Stars and Nucleogenesis. *Publications of the Astronomical Society of the Pacific*. 1957 Jun;69:201. Available from: <http://iopscience.iop.org/article/10.1086/127051>.
- [19] Guerrero C, Lerendegui-Marco J, Paul M, Tessler M, Heinitz S, Domingo-Pardo C, et al. Neutron Capture on the s -Process Branching Point Tm 171 via Time-of-Flight and Activation. *Physical Review Letters*. 2020 Oct;125(14):142701. Available from: <https://link.aps.org/doi/10.1103/PhysRevLett.125.142701>.
- [20] Käppeler F, Gallino R, Bisterzo S, Aoki W. The s process: Nuclear physics, stellar models, and observations. *Reviews of Modern Physics*. 2011 Apr;83(1):157-93. Available from: <https://link.aps.org/doi/10.1103/RevModPhys.83.157>.
- [21] Bernstein LA, Bleuel DL, Caggiano JA, Cerjan C, Fortner RJ, Gostic J, et al. Low Energy Neutron Measurements in High Energy Density Plasmas using the National Ignition Facility. *Plasma and Fusion Research*. 2014;9(0):4404101-1. Available from: https://www.jstage.jst.go.jp/article/pfr/9/0/9_4404101/_article.
- [22] Kappeler F, Beer H, Wisshak K. s-process nucleosynthesis-nuclear physics and the classical model. *Reports on Progress in Physics*. 1989 Aug;52(8):945-1013. Available from: <https://iopscience.iop.org/article/10.1088/0034-4885/52/8/002>.
- [23] Morita M. Nuclear Excitation by Electron Transition and Its Application to Uranium 235 Separation. *Progress of Theoretical Physics*. 1973 May;49(5):1574-86. Available from: <https://academic.oup.com/ptp/article-lookup/doi/10.1143/PTP.49.1574>.

- [24] Lynn JE, Jurney ET, Raman S. Direct and valence neutron capture by Li 7. *Physical Review C*. 1991 Aug;44(2):764-73. Available from: <https://link.aps.org/doi/10.1103/PhysRevC.44.764>.
- [25] Despotopoulos JD, Gharibyan N, Moody KJ, Yeamans C, Velsko C, Shaughnessy DA. Radiochemical capabilities for astrophysics experiments at the national ignition facility. *Frontiers in Physics*. 2022 Sep;10:944400. Available from: <https://www.frontiersin.org/articles/10.3389/fphy.2022.944400/full>.
- [26] Bao ZY, Beer H, Käppeler F, Voss F, Wissak K, Rauscher T. NEUTRON CROSS SECTIONS FOR NUCLEOSYNTHESIS STUDIES. *Atomic Data and Nuclear Data Tables*. 2000 Sep;76(1):70-154. Available from: <https://linkinghub.elsevier.com/retrieve/pii/S0092640X00908386>.
- [27] Rauscher T, Mohr P, Dillmann I, Plag R. OPPORTUNITIES TO CONSTRAIN ASTROPHYSICAL REACTION RATES FOR THE s -PROCESS VIA DETERMINATION OF THE GROUND-STATE CROSS-SECTIONS. *The Astrophysical Journal*. 2011 Sep;738(2):143. Available from: <https://iopscience.iop.org/article/10.1088/0004-637X/738/2/143>.
- [28] Tkalya EV. Nuclear excitation in atomic transitions (NEET process analysis). *Nuclear Physics A*. 1992 Mar;539(2):209-22. Available from: <https://linkinghub.elsevier.com/retrieve/pii/037594749290267N>.
- [29] Morel P, Daugas JM, Gosselin G, Méot V, Gogny D. Nuclear excitation by electronic processes: NEEC and NEET effects. *Nuclear Physics A*. 2004 Dec;746:608-12. Available from: <https://linkinghub.elsevier.com/retrieve/pii/S0375947404010656>.
- [30] Lindl JD, Amendt P, Berger RL, Glendinning SG, Glenzer SH, Haan SW, et al. The physics basis for ignition using indirect-drive targets on the National Ignition Facility. *Physics of Plasmas*. 2004 Feb;11(2):339-491. Available from: <https://pubs.aip.org/pop/article/11/2/339/260912/The-physics-basis-for-ignition-using-indirect>.
- [31] Atherton LJ, Moses EI, Carlisle K, Kilkenny J. The Ignition Target for the National Ignition Facility. Lawrence Livermore National Lab. (LLNL), Livermore, CA (United States); 2007. UCRL-CONF-229008. Available from: <https://www.osti.gov/biblio/909643>.
- [32] Yeamans CB, Kemp GE, Walters ZB, Whitley HD, McKenty PW, Garcia EM, et al. High yield polar direct drive fusion neutron sources at the National Ignition Facility. *Nuclear Fusion*. 2021 Apr;61(4):046031. Available from: <https://iopscience.iop.org/article/10.1088/1741-4326/abe4e6>.
- [33] Whitley HD, Kemp GE, Yeamans CB, Walters ZB, Blue BE, Garbett WJ, et al. Comparison of ablators for the polar direct drive exploding pusher platform. *High Energy Density Physics*. 2021 Mar;38:100928. Available from: <https://linkinghub.elsevier.com/retrieve/pii/S1574181821000057>.

- [34] Schmitt MJ, Bradley PA, Cobble JA, Fincke JR, Hakel P, Hsu SC, et al. Development of a polar direct-drive platform for studying inertial confinement fusion implosion mix on the National Ignition Facility. *Physics of Plasmas*. 2013 May;20(5):056310. Available from: <https://pubs.aip.org/pop/article/20/5/056310/109297/Development-of-a-polar-direct-drive-platform-for>.
- [35] Ellison CL, Whitley HD, Brown CRD, Copeland SR, Garbett WJ, Le HP, et al. Development and modeling of a polar-direct-drive exploding pusher platform at the National Ignition Facility. *Physics of Plasmas*. 2018 Jul;25(7):072710. Available from: <https://pubs.aip.org/pop/article/25/7/072710/319433/Development-and-modeling-of-a-polar-direct-drive>.
- [36] Yeamans C, Blue B. National Ignition Facility Neutron Sources. Lawrence Livermore National Lab. (LLNL), Livermore, CA (United States); 2018. LLNL-CONF-739397. Available from: <https://www.osti.gov/biblio/1458648>.
- [37] Shaughnessy DA, Moody KJ, Gharibyan N, Grant PM, Gostic JM, Torretto PC, et al. Radiochemical determination of Inertial Confinement Fusion capsule compression at the National Ignition Facility. *Review of Scientific Instruments*. 2014 Jun;85(6):063508. Available from: <https://pubs.aip.org/rsi/article/85/6/063508/356133/Radiochemical-determination-of-Inertial>.
- [38] Shaughnessy DA, Velsko CA, Jedlovec DR, Yeamans CB, Moody KJ, Tereshatov E, et al. The Radiochemical Analysis of Gaseous Samples (RAGS) apparatus for nuclear diagnostics at the National Ignition Facility (invited). *Review of Scientific Instruments*. 2012 Oct;83(10):10D917. Available from: <https://pubs.aip.org/rsi/article/83/10/10D917/359841/The-Radiochemical-Analysis-of-Gaseous-Samples-RAGS>.
- [39] Cerjan CJ, Bernstein L, Hopkins LB, Bionta RM, Bleuel DL, Caggiano JA, et al. Dynamic high energy density plasma environments at the National Ignition Facility for nuclear science research. *Journal of Physics G: Nuclear and Particle Physics*. 2018 Mar;45(3):033003. Available from: <https://iopscience.iop.org/article/10.1088/1361-6471/aa8693>.
- [40] NeSST: Neutron Scattered Spectra Tool;. Available from: <https://github.com/aidancrilly/NeSST>.
- [41] Crilly AJ, Appelbe BD, Mannion OM, Forrest CJ, Chittenden JP. The effect of areal density asymmetries on scattered neutron spectra in ICF implosions. *Physics of Plasmas*. 2021 Feb;28(2):022710. Available from: <https://pubs.aip.org/pop/article/28/2/022710/124738/The-effect-of-areal-density-asymmetries-on>.
- [42] Ge ZG, Zhao ZX, Xia HH, Zhuang YX, Liu TJ, Zhang JS, et al. The Updated Version of Chinese Evaluated Nuclear Data Library (CENDL-3.1). *Journal of the Korean Physical Society*. 2011 Aug;59(2(3)):1052-6. Available from: <http://www.jkps.or.kr/journal/DOIx.php?id=10.3938/jkps.59.1052>.

- [43] Ballabio L, Källne J, Gorini G. Relativistic calculation of fusion product spectra for thermonuclear plasmas. *Nuclear Fusion*. 1998 Nov;38(11):1723-35. Available from: <https://iopscience.iop.org/article/10.1088/0029-5515/38/11/310>.
- [44] Bosch HS, Hale GM. Improved formulas for fusion cross-sections and thermal reactivities. *Nuclear Fusion*. 1992 Apr;32(4):611-31. Available from: <https://iopscience.iop.org/article/10.1088/0029-5515/32/4/I07>.
- [45] Meaney KD, Kim YH, Herrmann HW, Geppert-Kleinrath H, Hoffman NM. Improved inertial confinement fusion gamma reaction history ^{12}C gamma-ray signal by direct subtraction. *Review of Scientific Instruments*. 2019 Nov;90(11):113503. Available from: <https://pubs.aip.org/rsi/article/90/11/113503/603086/Improved-inertial-confinement-fusion-gamma>.
- [46] Herrmann HW, Young CS, Mack JM, Kim YH, McEvoy A, Evans S, et al. ICF gamma-ray reaction history diagnostics. *Journal of Physics: Conference Series*. 2010 Aug;244(3):032047. Available from: <https://iopscience.iop.org/article/10.1088/1742-6596/244/3/032047>.
- [47] Crilly A. Simulation of nuclear observables in inertial confinement fusion experiments. Imperial College London; 2020.
- [48] Crilly AJ, Appelbe BD, McGlinchey K, Walsh CA, Tong JK, Boxall AB, et al. Synthetic nuclear diagnostics for inferring plasma properties of inertial confinement fusion implosions. *Physics of Plasmas*. 2018 Dec;25(12):122703. Available from: <https://pubs.aip.org/pop/article/25/12/122703/364054/Synthetic-nuclear-diagnostics-for-inferring-plasma>.
- [49] Edwards MJ, Lindl JD, Spears BK, Weber SV, Atherton LJ, Bleuel DL, et al. The experimental plan for cryogenic layered target implosions on the National Ignition Facility—The inertial confinement approach to fusion. *Physics of Plasmas*. 2011 May;18(5):051003. Available from: <https://pubs.aip.org/pop/article/18/5/051003/810066/The-experimental-plan-for-cryogenic-layered-target>.
- [50] Glenzer SH, Spears BK, Edwards MJ, Alger ET, Berger RL, Bleuel DL, et al. First implosion experiments with cryogenic thermonuclear fuel on the National Ignition Facility. *Plasma Physics and Controlled Fusion*. 2012 Apr;54(4):045013. Available from: <https://iopscience.iop.org/article/10.1088/0741-3335/54/4/045013>.
- [51] Herrmann HW, Langenbrunner JR, Mack JM, Cooley JH, Wilson DC, Evans SC, et al. Anomalous yield reduction in direct-drive deuterium/tritium implosions due to H_3e addition. *Physics of Plasmas*. 2009 May;16(5):056312. Available from: <https://pubs.aip.org/pop/article/16/5/056312/678097/Anomalous-yield-reduction-in-direct-drive>.
- [52] Lindl J, Landen O, Edwards J, Moses E, NIC Team. Review of the National Ignition Campaign 2009-2012. *Physics of Plasmas*. 2014 Feb;21(2):020501. Available from: <https://pubs.aip.org/aip/pop/article/106548>.

- [53] Kim Y, Herrmann HW, Hoffman NM, Schmitt MJ, Kagan G, McEvoy AM, et al. First observation of increased DT yield over prediction due to addition of hydrogen. *Physics of Plasmas*. 2021 Jan;28(1):012707. Available from: <https://pubs.aip.org/pop/article/28/1/012707/1059963/First-observation-of-increased-DT-yield-over>.
- [54] Quartemont NJ, Peterson G, Moran C, Samin A, Wang B, Yeomans C, et al. ATHENA: A unique radiation environment platform at the National Ignition Facility. *Nuclear Instruments and Methods in Physics Research Section A: Accelerators, Spectrometers, Detectors and Associated Equipment*. 2021 Nov;1016:165777. Available from: <https://linkinghub.elsevier.com/retrieve/pii/S0168900221007622>.
- [55] Quartemont N, Gharibyan N, Moody K, Bevins JE. Uranium integral fission product yields for a spectrally-shaped 14.1 MeV neutron source at the National Ignition Facility. *Applied Radiation and Isotopes*. 2021 Jul;173:109711. Available from: <https://linkinghub.elsevier.com/retrieve/pii/S0969804321001184>.
- [56] Zylstra Aritcher Auricane Oallahan Daker K, Braun T, et al. Record Energetics for an Inertial Fusion Implosion at NIF. *Physical Review Letters*. 2021 Jan;126(2):025001. Available from: <https://link.aps.org/doi/10.1103/PhysRevLett.126.025001>.